Supplementary Information

Intramolecular interactions of conjugated polymers mimic molecular chaperones to stabilize protein-polymer conjugates

Stefanie L. Baker[1,2], Aravinda Munasinghe[3], Hironobu Murata[2], Ping Lin[3], Krzysztof Matyjaszewski[4], Coray M. Colina[3,5] Alan J. Russell[1,2,4,6,7*]

[1]Department of Biomedical Engineering, Scott Hall 4N201, Carnegie Mellon University, 5000 Forbes Avenue, Pittsburgh, PA 15213, United States

[2]Center for Polymer-Based Protein Engineering, Carnegie Mellon University, 5000 Forbes Avenue, Pittsburgh, PA 15213, United States

[3]Department of Chemistry, 312 Leigh Hall, University of Florida, Gainesville, FL 32611, United States

[4]Department of Chemistry, Carnegie Mellon University, 4400 Fifth Avenue, Pittsburgh, PA 15213, United States

[5]Department of Materials Science and Engineering, University of Florida, Gainesville, FL 32611, United States

[6]Disruptive Health Technology Institute, Carnegie Mellon University, 5000 Forbes Avenue, Pittsburgh, PA 15213, United States

[7]Department of Chemical Engineering, Carnegie Mellon University, 5000 Forbes Avenue, Pittsburgh, PA 15213, United States

Supporting Information Discussion

Conjugate Characterization

The hydrodynamic diameters, as determined by dynamic light scattering, were reported in number distribution. Volume and intensity values are also often reported when using dynamic light scattering and can provide more insight into the composition of the sample. For example, native CT had number, volume, and intensity distribution diameters of 1.8 ± 0.5, 2.5 ± 1.2, and 5.9 ± 3.5 nm, respectively. Since the values were different, this implied that the protein was not perfectly homogenous. The same holds true for all conjugate hydrodynamic diameters. All conjugate hydrodynamic diameters were reported by number distribution.

Molecular Dynamics Simulations

The diameters for CT-pCBMA conjugates were validated by calculating the contour lengths of the polymers obtained from molecular simulations of the monomer multiplied by the DP plus the length of the initiator. Considering that the polymer chains are dispersed across the surface of the protein, the overall diameter of the conjugate was estimated. The lengths of initiator and monomer were approximately 6.2 Å and 2.6 Å, respectively. Therefore, for DPs of 10, 46, and 112, the contour lengths of each pCBMA chain, including the initiator, are approximately 3.2, 12.6, and 29.7 nm. Further, the atomistic dynamics simulation results showed that although the polymer chains were dispersed across the entire surface of CT and could vary in conformations depending on interactions with the protein surface, each other, and the solvent, a majority of the polymer chains were extended into the solvent. Therefore, the radii of gyrations and hydrodynamic diameters of the conjugates were expected to grow with the length of the polymer

chains. The average radius of gyration of CT, CT-pCBMA 10, CT-pQA 10, and CT-pSMA 14 obtained from atomistic dynamic simulations were 1.7, 2.7, 2.8, and 3.0 nm, respectively.

Supporting Information Figures

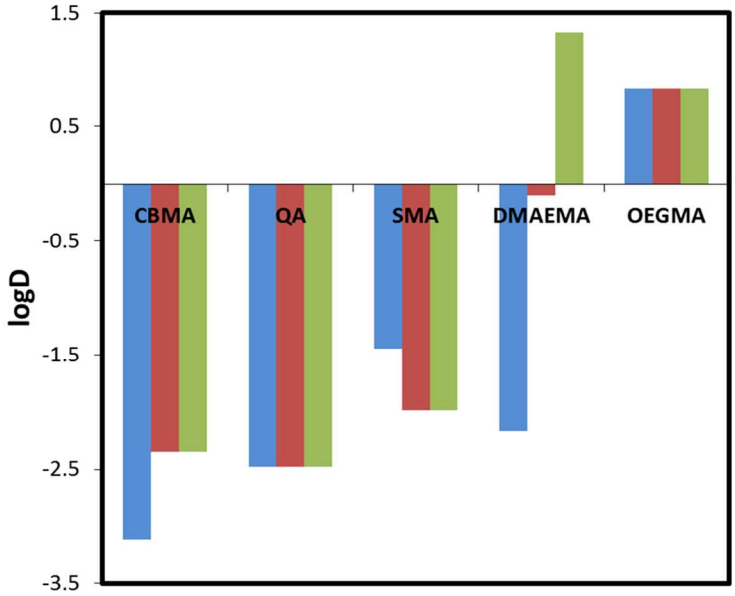

Figure S1. Monomer hydrophobicity as the distribution coefficient between octanol and water (logD) determined using ChemAxon at pH 1 (blue), 7 (red), and 12 (green). Hydrophobicity increases at pH 7 from QA < CBMA < SMA < DMAEMA < OEGMA.

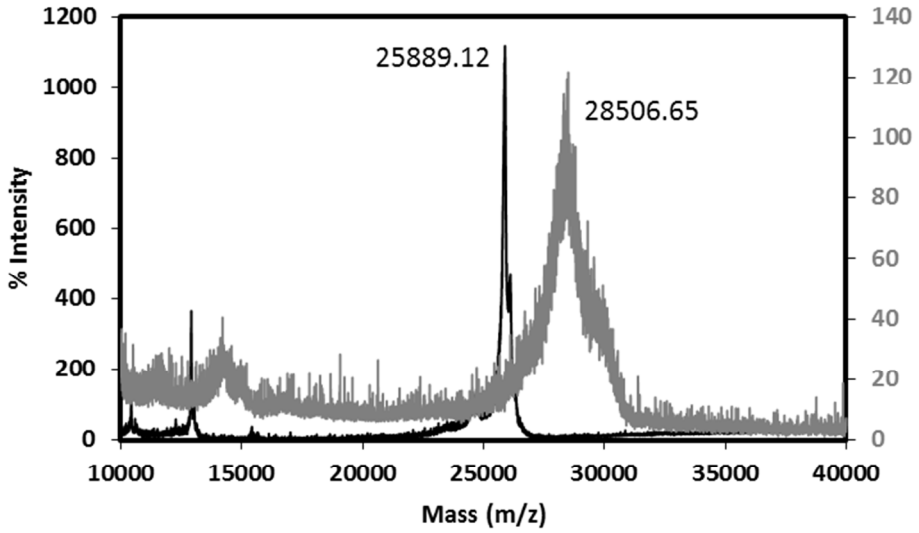

Figure S2. Matrix assisted laser desorption/ionization time-of-flight mass spectroscopy (MALDI-ToF MS) of native CT (black) and initiator modified CT (CT-Br, gray). The difference in m/z allows calculation of how many modification sites were achieved. The conjugated initiator adds a mass of 220.5 Da per modification site. Peak labels are in Da. CT was modified with 12 initiators for atom-transfer radical polymerization.

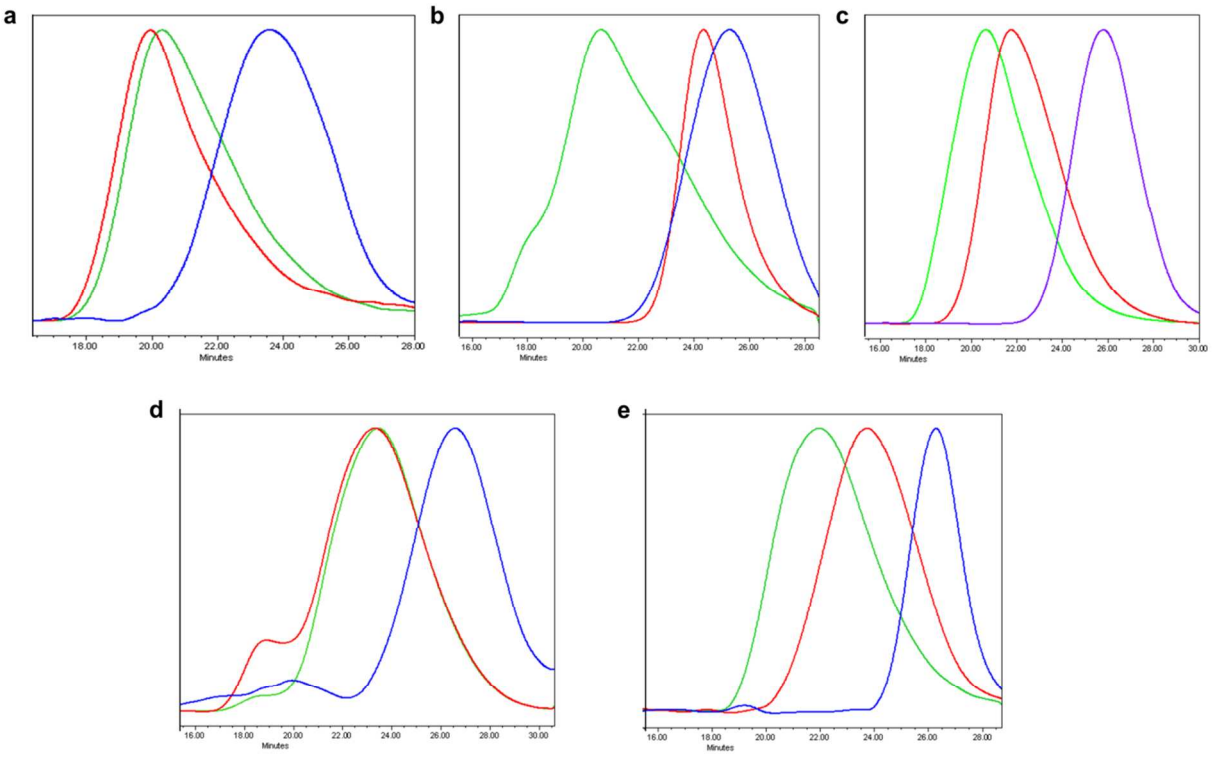

Figure S3. Gel permeation traces for cleaved polymer of varying molecular weights after acid hydrolysis for **a,** pCBMA **b,** pOEGMA **c,** pDMAEMA **d,** pQA **e,** pSMA. Molecular weights were relative to pullulan narrow standards.

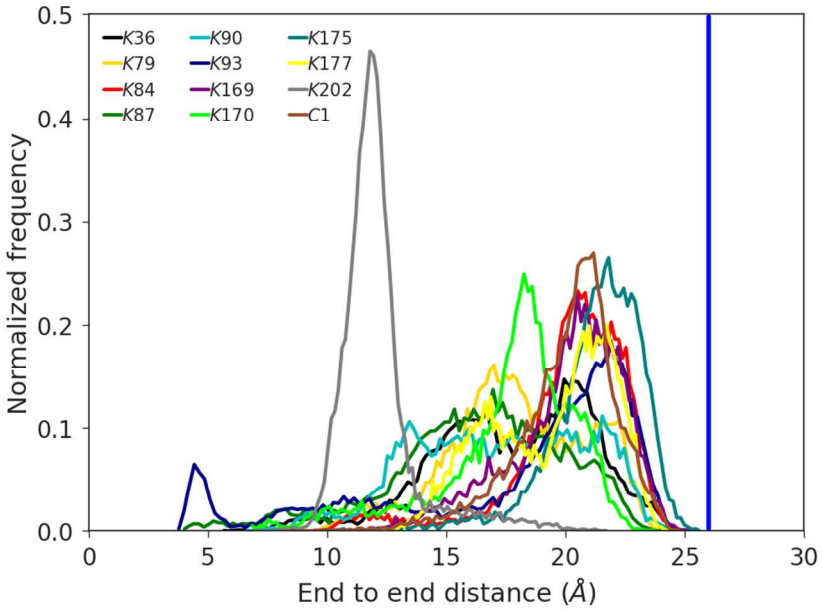

Figure S4. End to end distribution of each polymer in CT-pCBMA . pCBMA chains were highly flexible as seen by the large distribution in end-to-end distances between different polymer chains. pCBMA chains were shown to interact with the protein surface.

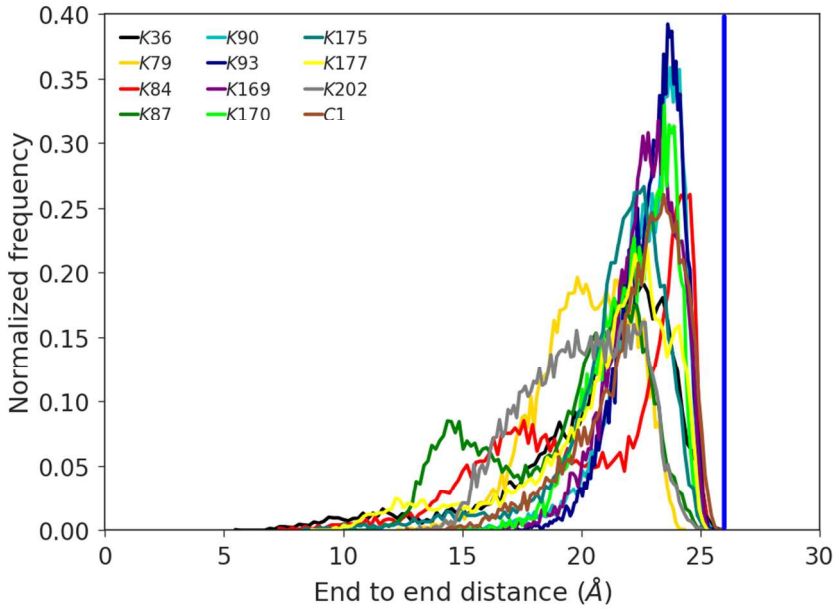

Figure S5. End to end distribution of each polymer in CT-pQA . The average end-to-end distances are different for different polymers. For example, the average end-to-end distances are ~15 and ~24 Å for K87 and K170, respectively. This indicated that pQA polymers were more flexible and were more likely to interact with the protein surface.

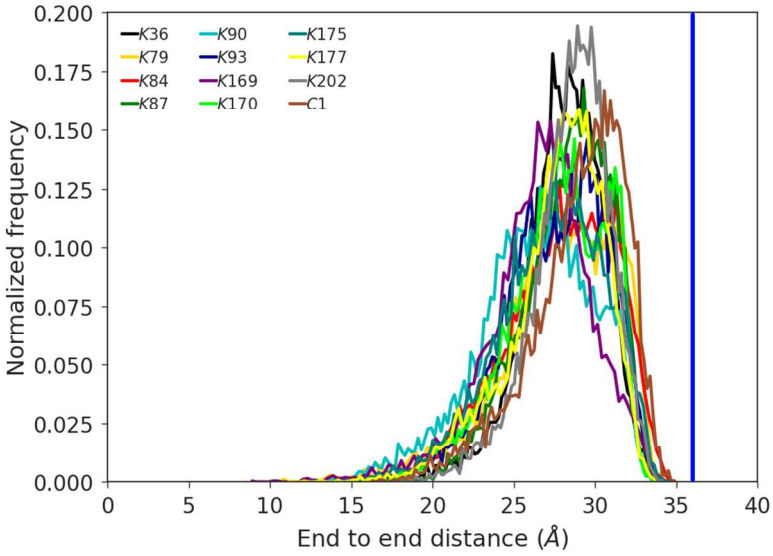

Figure S6. End to end distribution of each polymer in CT-pSMA. All chains had similarly high end-to-end distances indicating that the polymer chains were extended into solution, most likely due to unfavorable electrostatic interactions between sulfonate groups.

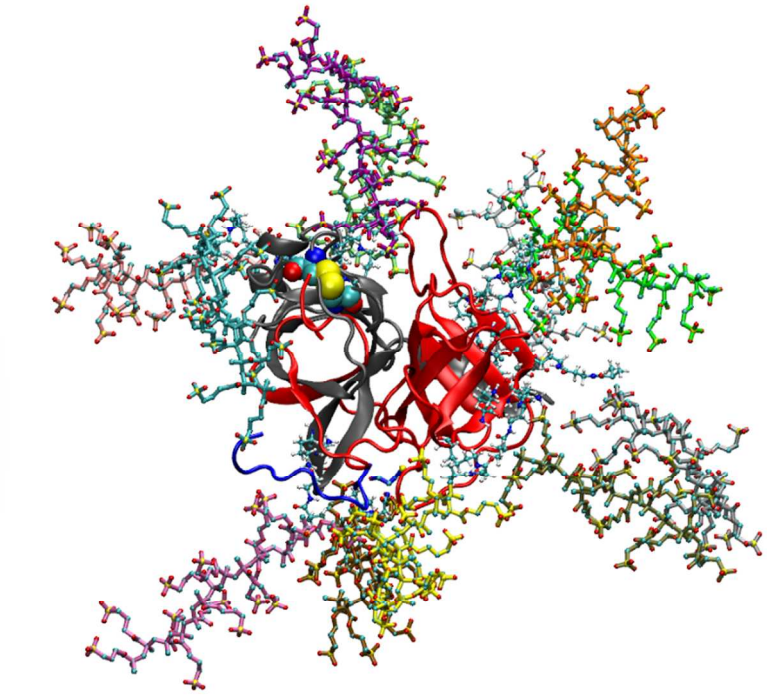

Figure S7. A snap shot of the CT-pSMA conjugate showing the pSMA chain conjugated to Lys170 (cyan), chain A (blue), B (grey) and C (red) of CT. The S1 binding pocket is near the two Cys residues in CPK representation.

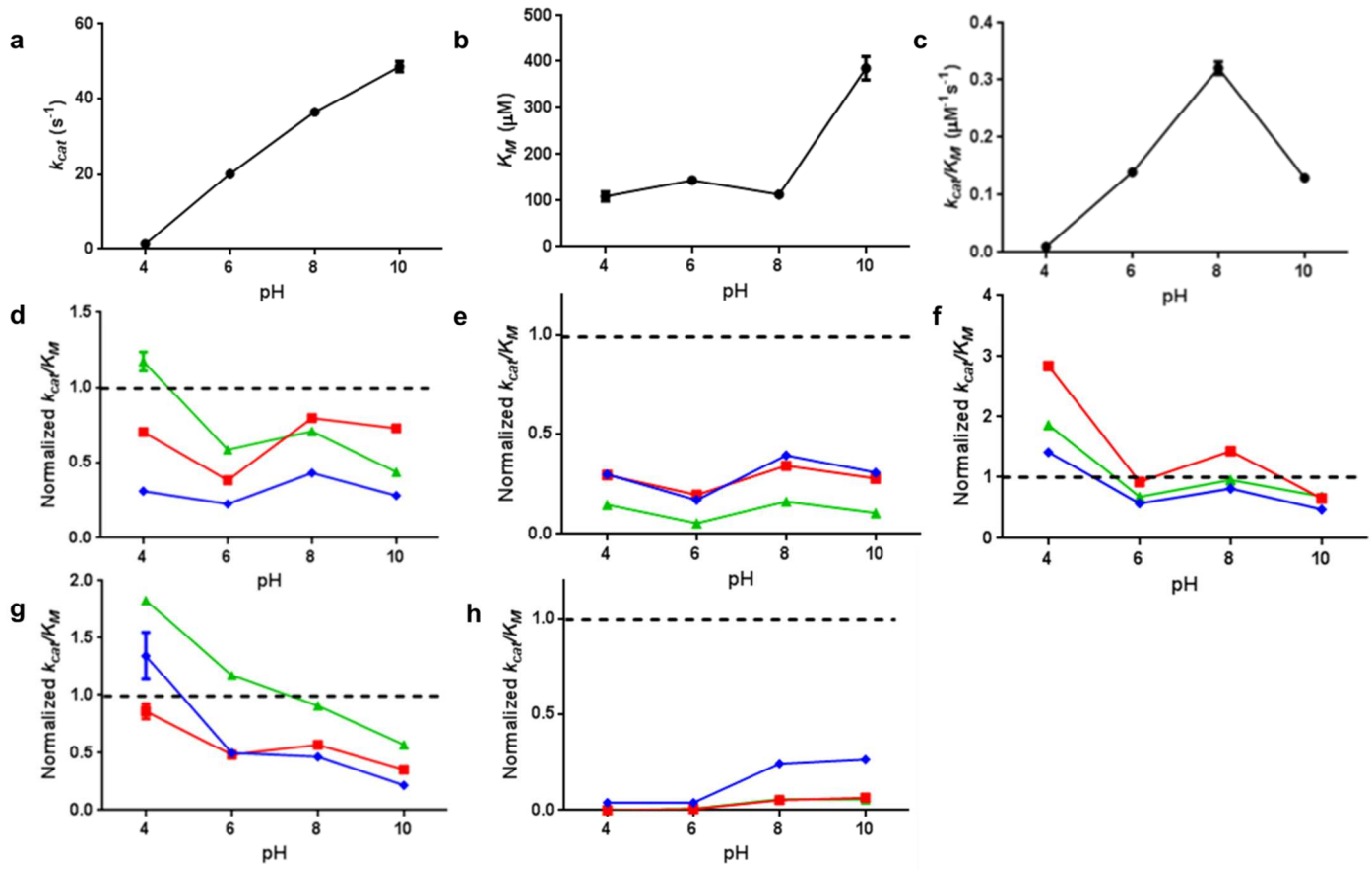

Figure S8. a, k_{cat}, s^{-1} of native CT. **b,** K_M, µM of native CT. Overall catalytic efficiency (k_{cat}/K_M, $\mu M^{-1} s^{-1}$) for **c,** native CT **d,** CT-pCBMA, **e,** CT-pOEGMA **f,** CT-pDMAEMA **g,** CT-pQA **h,** CT-pSMA. **d-h** are normalized to native CT at each pH. Normalized native CT (dashed black line), short length conjugates (blue diamonds), medium length conjugates (red squares), and long length conjugates (green triangles). Error bars represent the standard deviation from triplicate measurements.

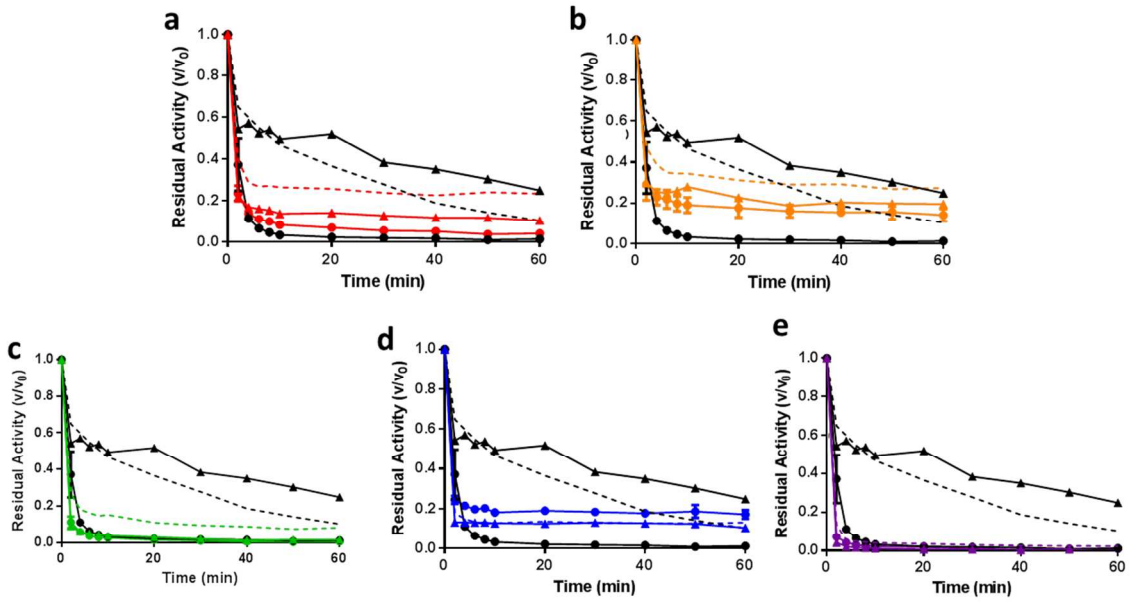

Figure S9. Residual activity measurements for stability of short length CT-conjugates at pH 1 while independently doping in 1.0 M NaCl or 10 v/v% dimethyl sulfoxide (DMSO) to disrupt electrostatic and hydrophobic interactions, respectively. In all plots **a-e,** native CT (dashed black line), native CT with NaCl (black circles), and native CT with DMSO (black triangles). **a,** CT-pCBMA (±) (red). **b,** CT-pOEGMA (0) (orange). **c,** CT-pQA (+) (green). **d,** CT-pSMA (-) (blue). **e,** CT-pDMAEMA (+/0) (purple). In all plots, stability of conjugates without NaCl or DMSO (colored dashed lines), conjugates with NaCl (colored circles), and conjugates with DMSO (colored triangles). The addition of NaCl and DMSO did not increase stability indicating an alternative mechanism for conjugate stabilization. Error bars represent standard error of the mean from triplicate measurements.

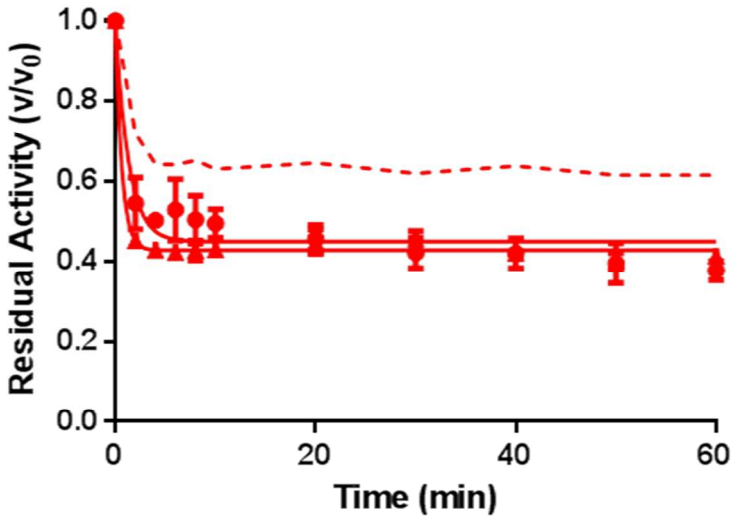

Figure S10. Residual activity measurements for stability of long length CT-pCBMA 112 at pH 1 while independently doping in 1.0 M NaCl or 10 v/v% dimethyl sulfoxide (DMSO) to disrupt electrostatic and hydrophobic interactions, respectively. NaCl and DMSO were also added in the refolding buffer (pH 8, sodium phosphate). CT-pCBMA 112 at pH 1 (red dashed line), CT-pCBMA 112 incubated with 1.0 M NaCl and refolded in buffer with 1.0 M NaCl (red circles), and CT-pCBMA 112 incubated with 10 v/v% DMSO and refolded in buffer with 10 v/v% DMSO (red triangles). Error bars represent standard error of the mean from triplicate measurements.

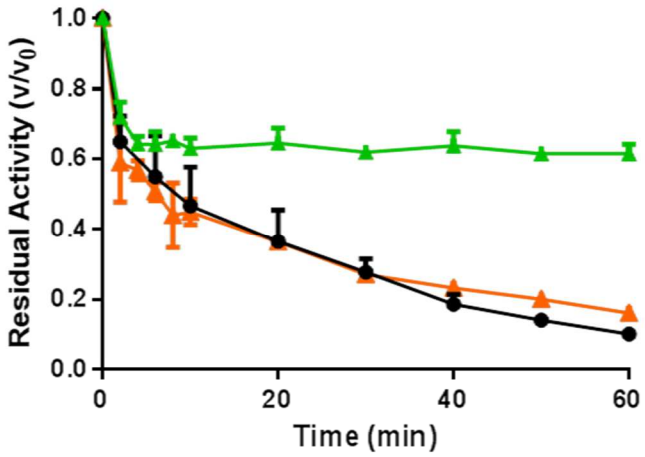

Figure S11. Residual activity measurements for stability of native CT (black circles), CT-pCBMA 112 (green triangles), and an equal mixture of native CT plus CT-pCBMA 112 (orange triangles). Stabilization is not due to intermolecular interactions between a conjugate and native protein. Error bars represent standard error of the mean from triplicate measurements.

Supporting Information Tables

Table S1. Atom-transfer radical polymerization conditions for conjugate synthesis. Reactions were performed at 4 °C to prevent CT autolysis. Increasing chain length was achieved by increasing the initiator to monomer ratio ([I]:[M]).

Conjugate	Catalyst	Ligand	Final Concentration (mM) [M]:[I]:[Cu(I)]:[Cu(II)]:[L]	Reaction Time (h)
CT-pDMAEMA$_{9}$	Cu(I)Cl	HMTETA	14 : 1.15 : 5 : 0 : 5	18
CT-pDMAEMA$_{46}$	Cu(I)Cl	HMTETA	115 : 1.15 : 5 : 0 : 5	18
CT-pDMAEMA$_{89}$	Cu(I)Cl	HMTETA	230 : 1.15 : 5 : 0 : 5	18
CT-pSMA$_{14}$	Cu(II)Br + NaAsc (1.21 mM)	HMTETA	25 : 1 : 0 : 5 : 12	2
CT-pSMA$_{48}$	Cu(II)Br + NaAsc (1.21 mM)	HMTETA	100 : 1 : 0 : 5 : 12	2
CT-pSMA$_{113}$	Cu(II)Br + NaAsc (1.21 mM)	HMTETA	175 : 1 : 0 : 5 : 12	2
CT-pQA$_{10}$	Cu(I)Br	HMTETA	25 : 0.72 : 1 : 0 : 1.2	2
CT-pQA$_{43}$	Cu(I)Br	HMTETA	111 : 0.72 : 1 : 0 : 1.2	2
CT-pQA$_{89}$	Cu(I)Br	HMTETA	175 : 0.72 : 1 : 0 : 1.2	2
CT-pOEGMA$_{9}$	Cu(II)Br + NaAsc (1.21 mM)	HMTETA	12 : 1 : 0 : 5 : 12	4
CT-pOEGMA$_{53}$	Cu(I)Cl/Cu(II)Cl	bpy	125 : 1 : 1.1 : 9.9 : 24.1	18
CT-pOEGMA$_{97}$	Cu(II)Br + NaAsc (1.21 mM)	HMTETA	220 : 1 : 0 : 5 : 12	4
CT-pCBMA$_{10}$	Cu(I)Br	HMTETA	30 : 1 : 2 : 0 : 2.4	2
CT-pCBMA$_{46}$	Cu(I)Br	HMTETA	125 : 1 : 2 : 0 : 2.4	2
CT-pCBMA$_{112}$	Cu(I)Br	HMTETA	220 : 1 : 2 : 0 : 2.4	2

Table S2. Kinetic rates of residual activity measurements for conjugates at pH 1 and pH 12. Rates were calculated using non-linear fitting in GraphPad. Error bars are standard error of the mean from triplicate measurements.

	pH 1			*pH 12*	
	k_{fast} (min^{-1})	k_{slow} (min^{-1})	Plateau Value	k_{fast} (min^{-1})	k_{slow} (min^{-1})
Native CT	1.128 ± 0.666	0.030 ± 0.005	-	0.103 ± 0.046	0.0101 ± 0.178
CT-Br	1.689 ± 0.049	-	-	0.521 ± 0.049	0.051 ± 0.034
CT-pCBMA 10	0.804 ± 0.043	-	0.248 ± 0.005	0.368 ± 0.055	0.023 ± 0.015
CT-pCBMA 46	0.999 ± 0.038	-	0.051 ± 0.003	0.407 ± 0.047	0.038 ± 0.019
CT-pCBMA 112	0.726 ± 0.089	-	0.630 ± 0.006	0.386 ± 0.077	0.020 ± 0.023
CT-pOEGMA 9	0.647 ± 0.045	-	0.308 ± 0.007	0.358 ± 0.045	0.034 ± 0.016
CT-pOEGMA 53	3.044 ± 4.554	-	0.358 ± 0.004	0.528 ± 0.120	0.093 ± 0.044
CT-pOEGMA 97	2.704 ± 2.076	-	0.249 ± 0.004	0.399 ± 0.024	0.063 ± 0.020
CT-pQA 10	0.814 ± 0.055	-	0.115 ± 0.007	0.167 ± 0.149	0.020 ± 0.193
CT-pQA 43	0.985 ± 0.046	-	0.074 ± 0.004	0.179 ± 0.057	0.025 ± 0.081
CT-pQA 89	1.055 ± 0.130	-	0.493 ± 0.005	0.138 ± 0.035	0.019 ± 0.006
CT-pDMAEMA 9	1.113 ± 0.036	-	0.034 ± 0.002	0.836 ± 0.061	0.078 ± 0.024
CT-pDMAEMA 46	1.037 ± 0.094	-	0.165 ± 0.007	0.697 ± 0.045	0.065 ± 0.018
CT-pDMAEMA 89	1.171 ± 0.050	-	0.063 ± 0.003	0.748 ± 0.052	0.064 ± 0.015
CT-pSMA 14	1.447 ± 0.059	-	0.132 ± 0.002	1.109 ± 0.074	0.095 ± 0.016
CT-pSMA 48	5.037 ± 270	-	0.180 ± 0.006	1.813 ± 4.631	0.305 ± 0.138
CT-pSMA 113	1.933 ± 0.453	-	0.295 ± 0.004	0.609 ± 0.246	0.087 ± 0.136

Supporting Information References

1. Rodríguez-Martínez, J. A. *et al.* Stabilization of α-chymotrypsin upon PEGylation correlates with reduced structural dynamics. *Biotechnol. Bioeng.* **101,** 1142–1149 (2008).

2. Farhadian, S. *et al.* Molecular aspects of the interaction of spermidine and alpha-chymotrypsin. *Int. J. Biol. Macromol.* **92,** 523–532 (2016).

3. Cummings, C. S. *et al.* Design of stomach acid-stable and mucin binding-enzyme polymer conjugates. *Biomacromolecules* acs.biomac.6b01723 (2017). doi:10.1021/acs.biomac.6b01723

4. Gaertner, H. F. & Puigserver, A. J. Increased activity and stability of poly(ethylene glycol)-modified trypsin. *Enzyme Microb. Technol.* **14,** 150–155 (1992).

5. Treetharnmathurot, B. *et al.* Dextrin-trypsin and ST-HPMA-trypsin conjugates: Enzyme activity, autolysis and thermal stability. *Int. J. Pharm.* **373,** 68–76 (2009).

6. Nodake, Y. & Yamasaki, N. Some properties of a macromolecular conjugate of lysozyme prepared by modification with a monomethoxypolyethylene glycol derivative. *Biosci. Biotechnol.* **8451,** (2000).

7. Lucius, M. *et al.* Investigating the Impact of Polymer Functional Groups on the Stability and Activity of Lysozyme-Polymer Conjugates. *Biomacromolecules* **17,** 1123–1134 (2016).

8. Morgenstern, J., Baumann, P., Brunner, C. & Hubbuch, J. Effect of PEG molecular weight and PEGylation degree on the physical stability of PEGylated lysozyme. *Int. J. Pharm.* **519,** 408–417 (2017).

9. Cao, L. *et al.* Protein–polymer conjugates prepared via host–guest interactions: effects of the conjugation site, polymer type and molecular weight on protein activity. *Polym. Chem.* **7,** 5139–5146 (2016).

10. Yang, W. *et al.* Improvement of Site-Directed Protein-Polymer Conjugates: High Bioactivity and Stability Using a Soft Chain-Transfer Agent. *ACS Appl. Mater. Interfaces* **8,** 15967–15974 (2016).

11. Mu, Q., Hu, T. & Yu, J. Molecular Insight into the Steric Shielding Effect of PEG on the Conjugated Staphylokinase: Biochemical Characterization and Molecular Dynamics Simulation. *PLoS One* **8,** 1–10 (2013).

12. García-Arellano, H., Valderrama, B., Saab-Rincón, G. & Vazquez-Duhalt, R. High temperature biocatalysis by chemically modified cytochrome c. *Bioconjug. Chem.* **13,** 1336–1344 (2002).

13. Yang, C., Lu, D. & Liu, Z. How PEGylation enhances the stability and potency of insulin: A molecular dynamics simulation. *Biochemistry* **50,** 2585–2593 (2011).

14. Pandey, B. K. *et al.* Impact of site-specific PEGylation on the conformational stability and folding rate of the Pin WW domain depends strongly on PEG oligomer length. *Bioconjug. Chem.* **24,** 796–802 (2013).

15. Natalello, A. *et al.* Biophysical characterization of Met-G-CSF: Effects of different site-specific mono-pegylations on protein stability and aggregation. *PLoS One* **7,** 1–9 (2012).

16. Plesner, B., Westh, P. & Nielsen, A. D. Biophysical characterisation of GlycoPEGylated recombinant human factor VIIa. *Int. J. Pharm.* **406,** 62–68 (2011).